Electronic Supplementary Material (ESI) for Physical Chemistry Chemical Physics.

[Supporting Information]

Pore Engineering of Carbonized Porous Aromatic Framework (PAF-1): Supercapacitors Application

Yanqiang Li,[a] Soumyajit Roy, [c] Teng Ben,[b] Shixian Xu, [a] Shilun Qiu*[a]*

[a] *State Key Laboratory of Inorganic Synthesis & Preparative Chemistry, Jilin University, Changchun 130012, China.* [b] *Department of Chemistry, Jilin University, Changchun, 130012, China;* [c] *EFAML, Materials Science Center, Department of Chemical Sciences, IISER-Kolkata, Mohanpur 741252, India.*

*To whom correspondence should be addressed. E-mail: tben@jlu.edu.cn; sqiu@jlu.edu.cn.

Table of Contents

1. Synthesis of PAF-1 and carbonized samples

PAF-1 was synthesized according to our previous report. The obtained white powder was heated in a furnace tube at a ramp rate of 2 ^{o}C min^{-1} to 750 ^{o}C in high pure (99.999%) nitrogen atmosphere or carbon dioxide and hold for 60 min to produce carbonized samples N_2-PAF-1 and CO_2-PAF-1. For KOH and NaOH activation, 100 mg of PAF-1 was impregnated with KOH solution (400 mg in 95 % ethanol), followed by an evaporation in nitrogen atmosphere. The activation was carried out by heating the sample in a furnace tube at a ramp rate of 2 ^{o}C min^{-1} to the final temperature and hold for 60 min. After cooled in flowing nitrogen, the resulting mixture was washed with 2 M HCl and lots of water to neutral. The activated samples ware denoted as K-PAF-1 and Na-PAF-1.

2. Characterization

Fourier transform infrared spectroscopy (FTIR). The FTIR spectra (KBr, Aldrich) were measured using a SHIMADZU IRAFFINITY-1 Fourier transform infrared spectrometer. Samples were packed firmly to get transparent films.

Power X-ray diffraction (PXRD) measurements. The PXRD measurements were performed on a Riguku D/MAX2550 diffractometer using Cu-Ka radiation, 35 kV, 25 mA with scanning rate of 10° min^{-1} (2θ).

Raman spectra. Raman spectra of the carbonized PAF-1s were measured by using Renishaw inVia Raman spectrometer, with the 514.5 nm line of an Ar ion laser as the excitation. The data was recorded from 1000-2000 cm^{-1}.

Thermogravimetric analysis (TGA). The thermogravimetric analysis (TGA) was performed using a SHIMADZU DTG-60 thermal analyzer system at the heating rate of 10 ^{o}C min^{-1} to 800 ^{o}C in dried air atmosphere and the air flow rate was 30 mL min^{-1}.

Nitrogen sorption measurements. Nitrogen sorption experiments were performed at 77 K up to 1 bar using a manometer sorption analyzer Autosorb iQ MP (Quantachrome Instruments). Before sorption analysis, the sample was evacuated at 200 °C for 10 h using a turbo molecular vacuum pump. Specific surface areas were calculated from nitrogen adsorption data by multipoint BET analysis. Pore size distributions were calculated from the N_2 adsorption isotherms using quenched solid density functional theory (QSDFT, nitrogen on carbon, slit pore) method which gives the least fitting error

3. Electrochemistry measurement

The working electrodes were prepared by grinding porous carbon (85 wt %, about 40 mg), acetylene black (10 wt %), and polytetrafluoroethylene (5 wt % PTFE, 60 wt % in water, diluted to 6 wt % before use) in a mortar and made into a film about 10 cm^2. The measured thickness of the electrode membrane was about xx μ m. The film was dried at

120 ^{o}C for 24 h under vacuum and was cut into square about 1 cm^{2}. Then it was pressed on nickel foam under 10 MPa. The typical mass load of the electrode was about 5 mg cm^{-2}. Cyclic voltammograms (CV), galvanostatic charge-discharge curves, and Nyquist plots were collected on a CHI660D electrochemical workstation. The electrochemical experiments were carried out using a three-electrode cell, employing platinum as the counter electrode; Hg/HgO electrodes (in 6.0 M KOH) or Ag/AgCl electrodes (for organic electrolytes) as reference electrodes, respectively. The specific capacitance derived from the CV measurement is calculated using the following eqution:

$$C = \frac{1}{m\,\upsilon(V_c - V_a)} \int_{V_a}^{V_c} I(V)\mathrm{d}V \qquad (1)$$

where C is the specific capacitance, m is the mass of electrode material, υ represents the scan rate, V_c and V_a refer to the high and low potential limit of the CV test, and I is the instant current on CV curves..

The gravimetric capacitance was calculated on the basis of the charge-discharge profile according to

$$C = \frac{I\Delta t}{m\Delta V} \qquad (2)$$

where I refers to the discharge current (A), and Δt represents the discharge time (s), m is the mass of electrode material (g), ΔV is the range of charge-discharge voltage (V).

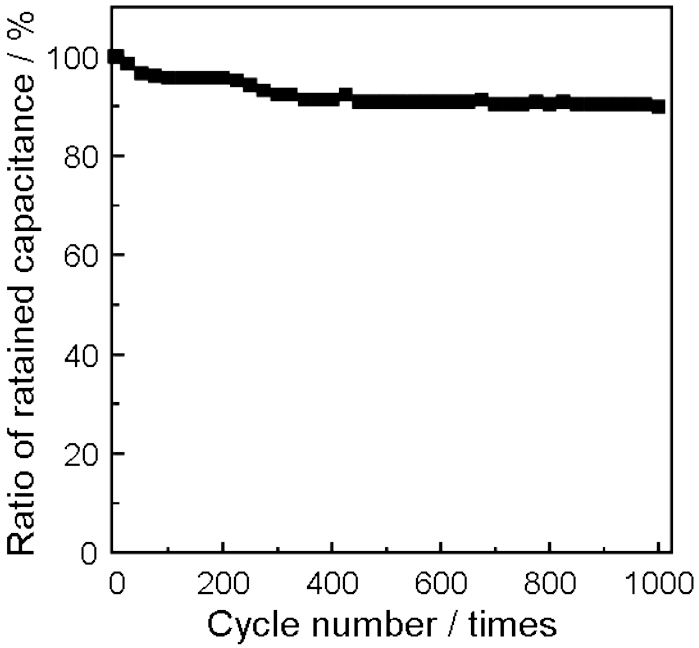

Figure S1. Cycle performance of K-PAF-1 in KOH elentrolyte.

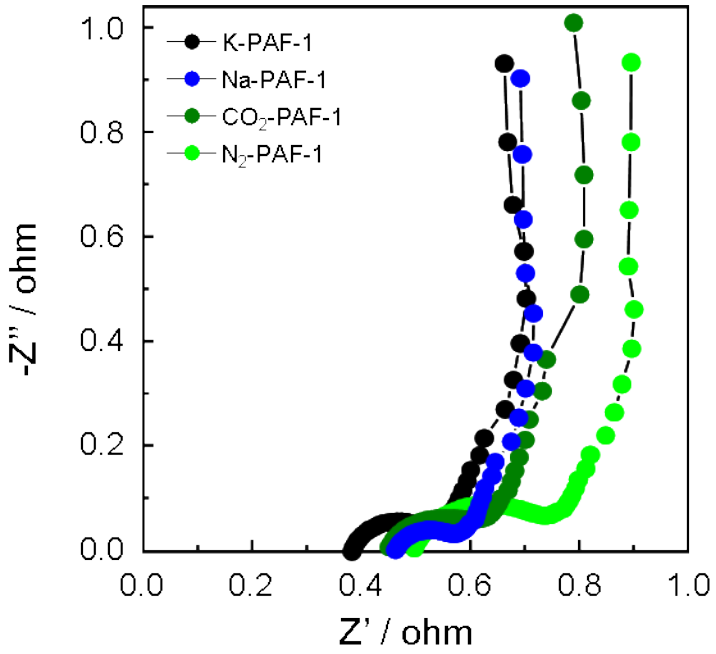

Figure S2. Enlarged Nyquist plots of carbonized PAF-1 in 6 M KOH.

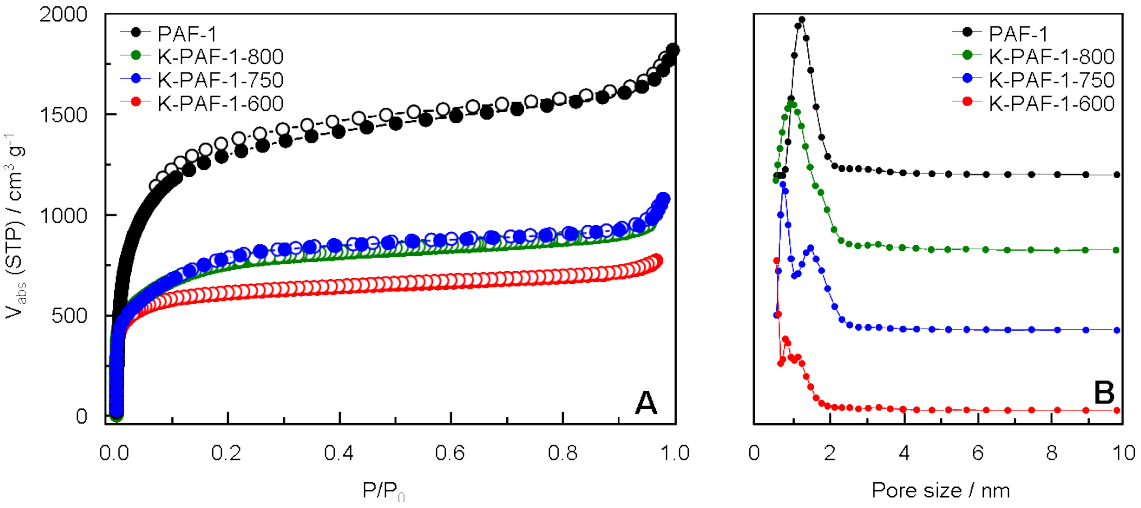

Figure S3. N_2 sorption and pore size distribution of PAF-1 and KOH activated samples at different temperatures.

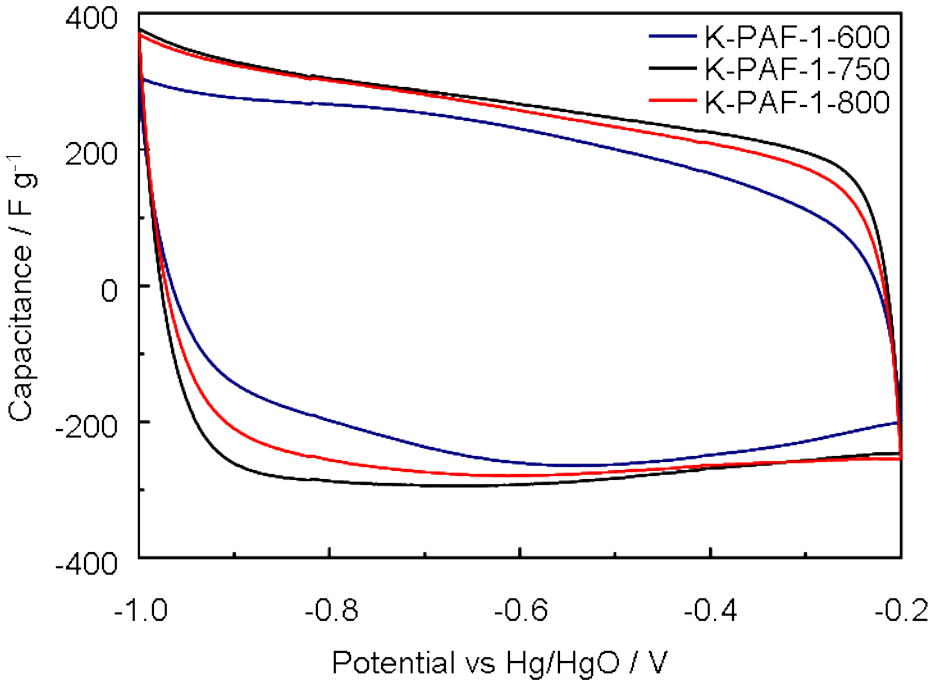

Figure S4. CV curves of K-PAF-1-600, K-PAF-1-750, K-PAF-1-800 at a scan rate of 0.05 V s^{-1} in 6 M KOH.

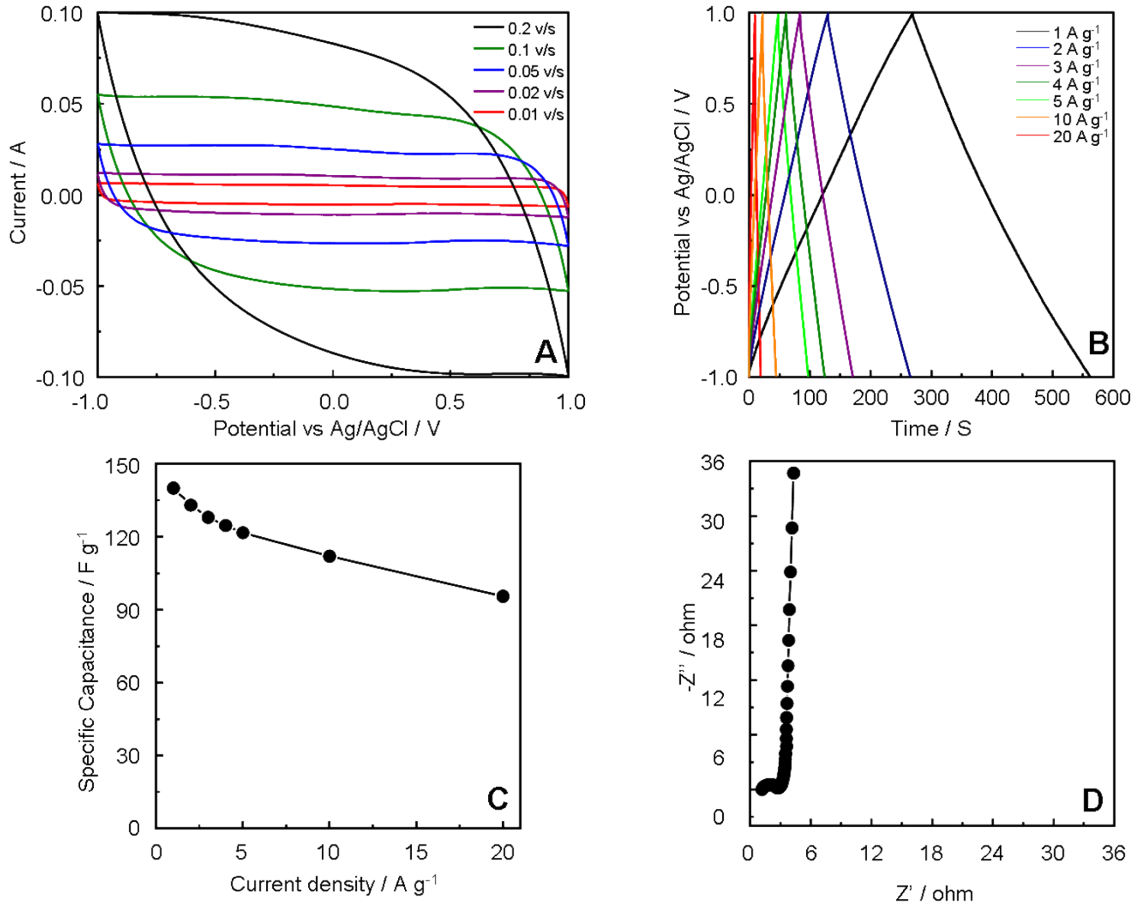

Figure S5. (A) CV curves of K-PAF-1 in $TEABF_4$; (B) galvanostatic charge–discharge curves of K-PAF-1 at different current density ; (C) capacitance versus current of K-PAF-1; (D) Nyquist plots (frequency ranges from 10^5 to 10^{-2} Hz) of K-PAF-1 in $TEABF_4$.

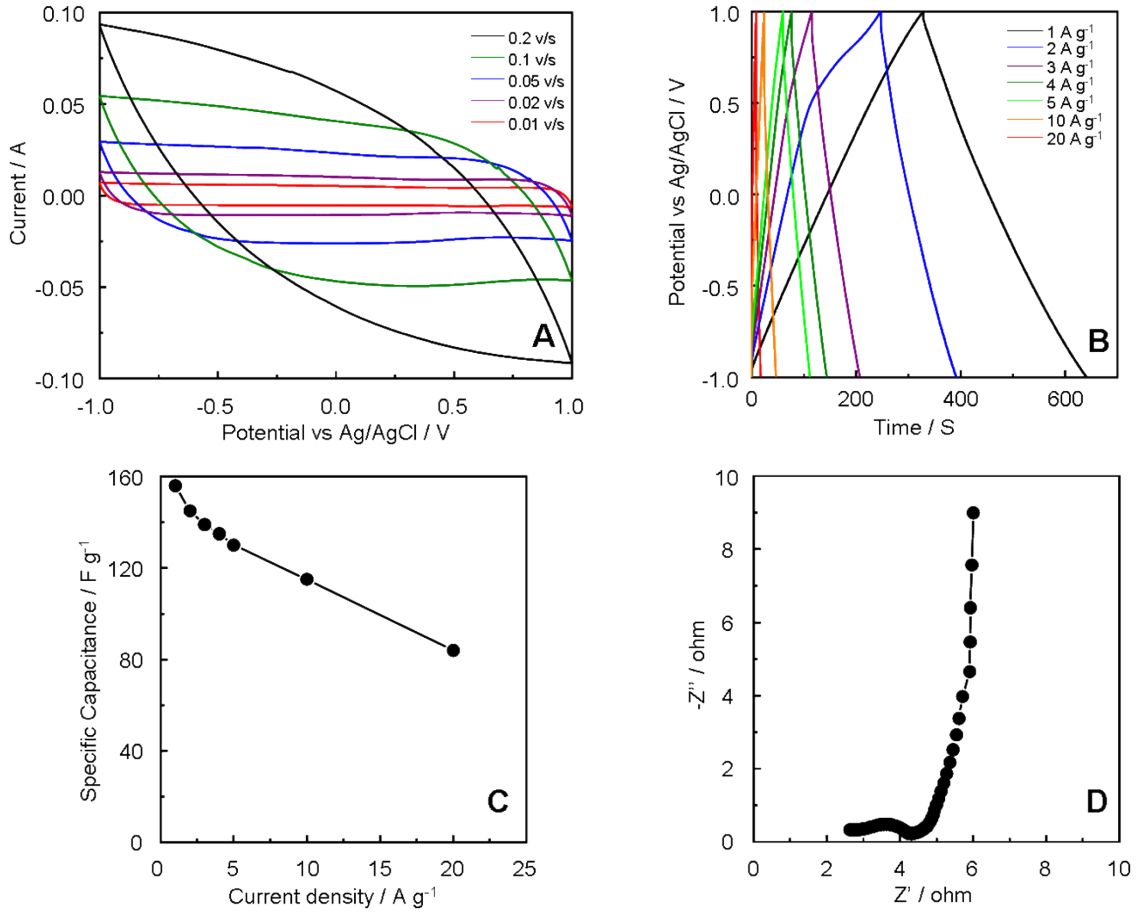

Figure S6. (A) CV curves of K-PAF-1; (B) galvanostatic charge–discharge curves of K-PAF-1 at different current density ; (C) capacitance versus current of K-PAF-1; (D) Nyquist plots (frequency ranges from 10^5 to 10^{-2} Hz) of K-PAF-1 in $EMImBF_4$.

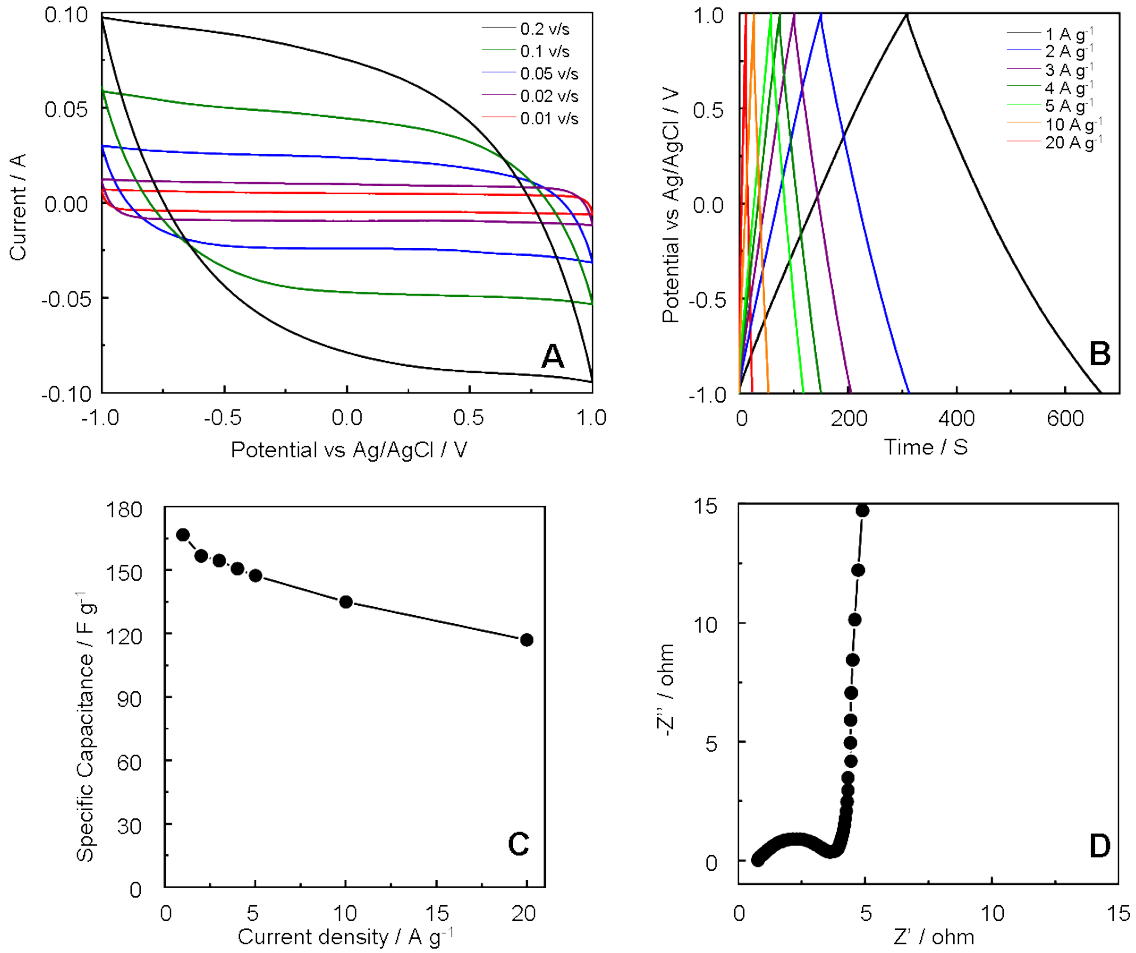

Figure S7. (A) CV curves of K-PAF-1; (B) galvanostatic charge–discharge curves of K-PAF-1 at different current density ; (C) capacitance versus current of K-PAF-1; (D) Nyquist plots (frequency ranges from 10^5 to 10^{-2} Hz) of K-PAF-1 in $BMImBF_4$.

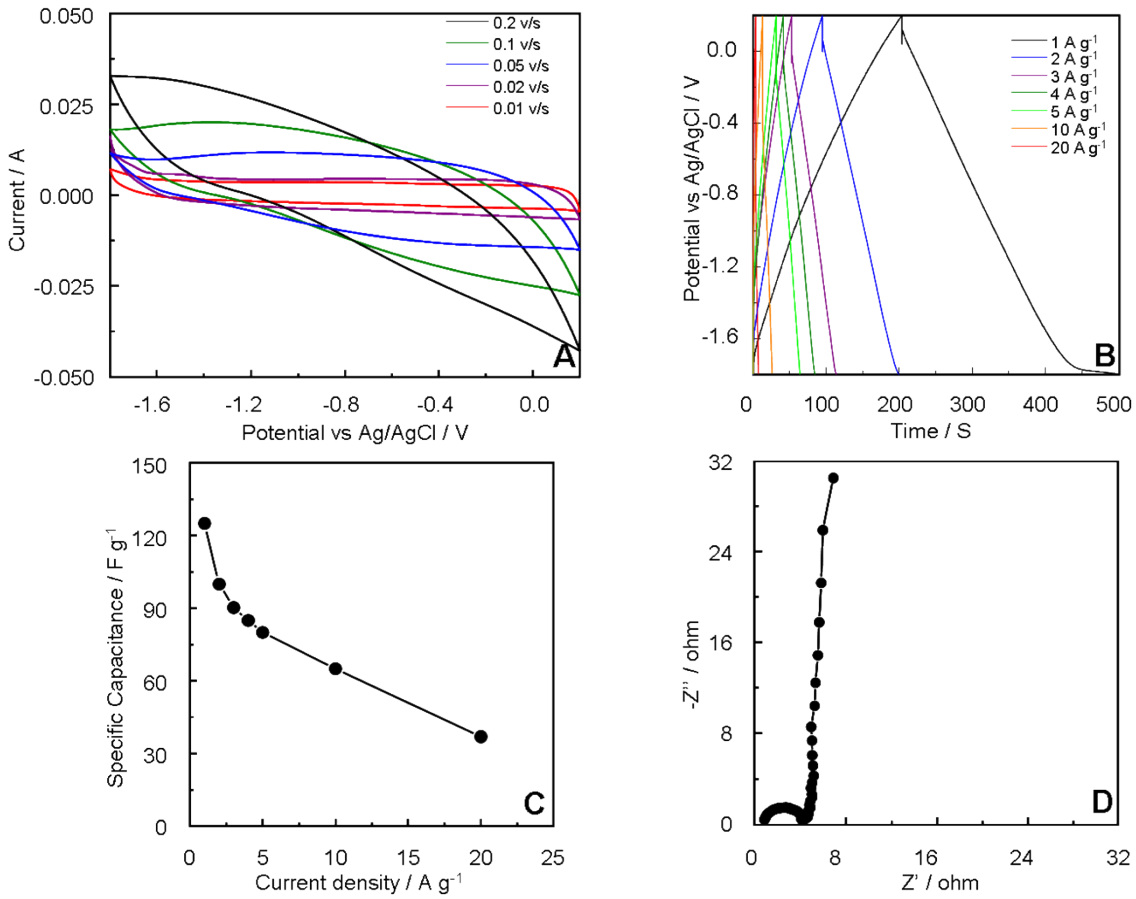

Figure S8. (A) CV curves of K-PAF-1; (B) galvanostatic charge–discharge curves of K-PAF-1 at different current density ; (C) capacitance versus current of K-PAF-1; (D) Nyquist plots (frequency ranges from 10^5 to 10^{-2} Hz) of K-PAF-1 in $TBABF_4$.

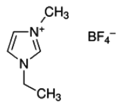

Equation	y = a + b*x		
Adj. R-Square	0.98555		
		Value	Standard Error
D	Intercept	157.31953	1.30828
D	Slope	-40.24593	2.17587

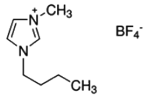

Equation	y = a + b*x		
Adj. R-Square	0.98982		
		Value	Standard Error
D	Intercept	176.82348	1.13195
D	Slope	-41.55273	1.8826

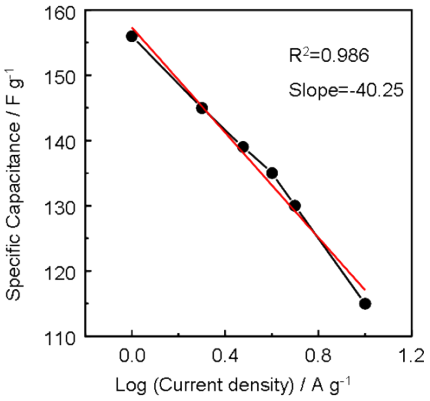

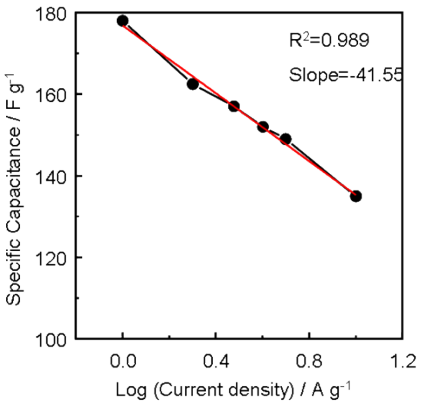

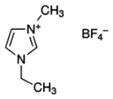

Equation	y = a + b*x		
Adj. R-Square	0.98555		
		Value	Standard Error
D	Intercept	157.31953	1.30828
D	Slope	-40.24593	2.17587

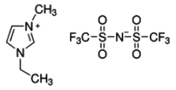

Equation	y = a + b*x		
Adj. R-Square	0.99275		
		Value	Standard Error
D	Intercept	201.31583	1.75929
D	Slope	-76.61415	2.92596

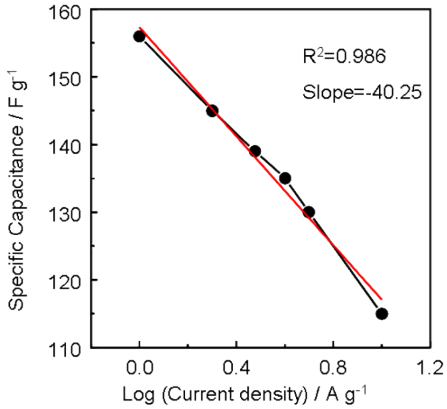

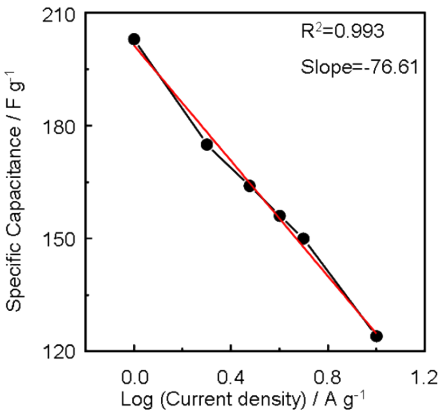

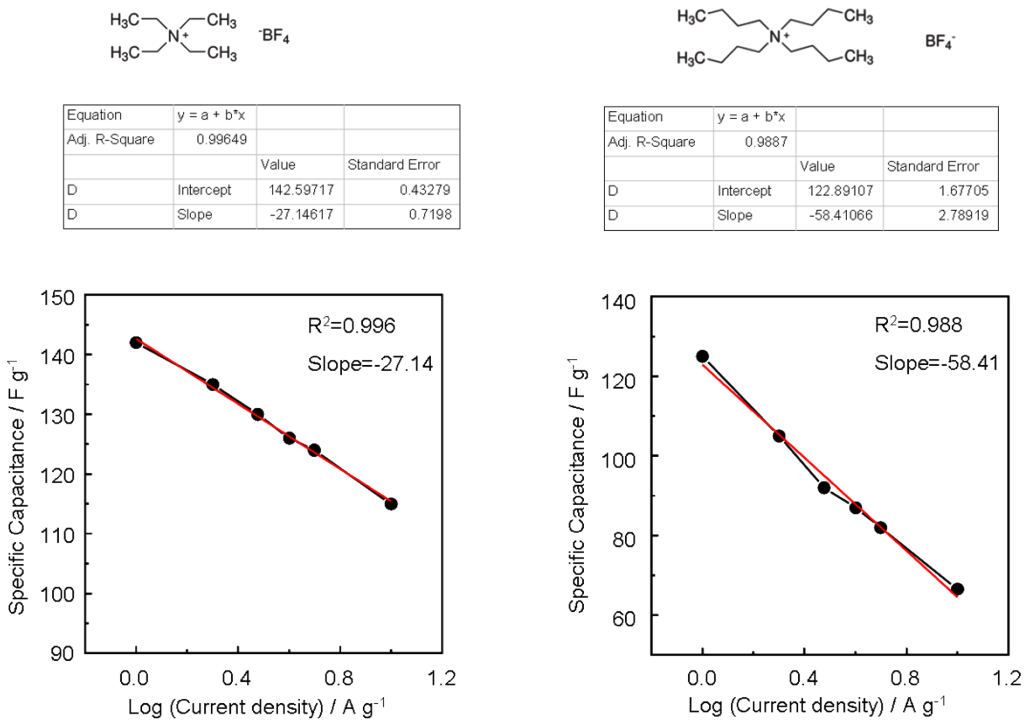

Figure S9. Analysis of capacitance decreasing trend with increasing current density.

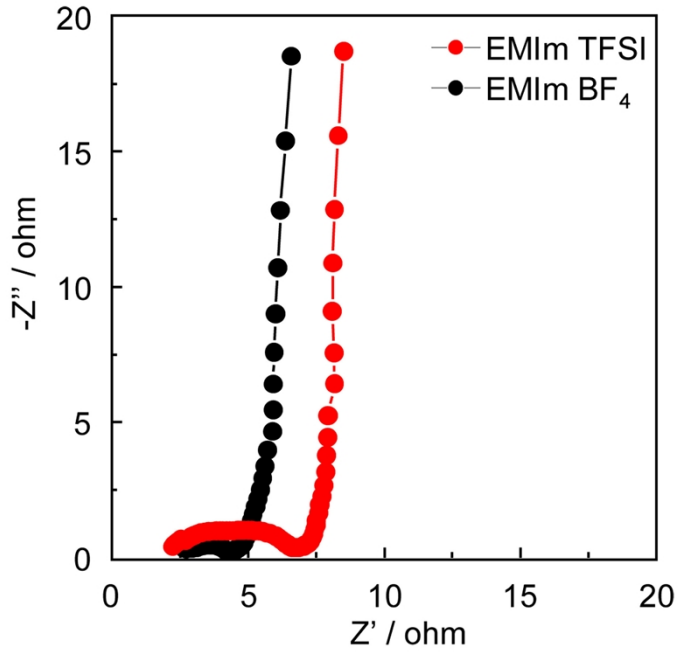

Figure S10. Nyquist plot of K-PAF-1 in EMIm TFSI and EMIm BF_4..

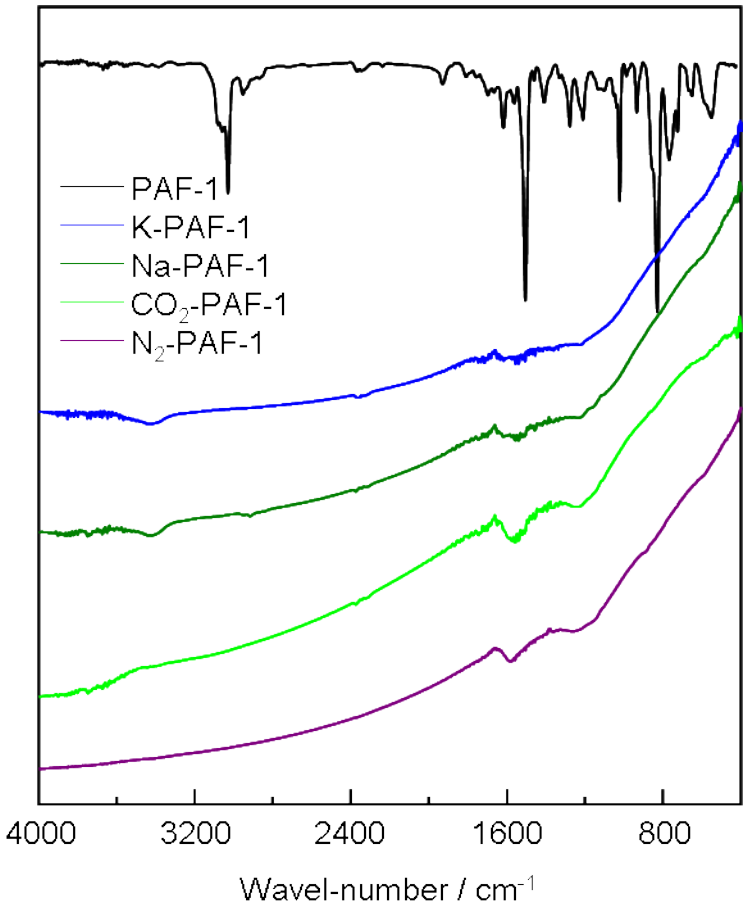

Figure S11. FTIR sprctra of PAF-1 and the carbonized samples. The disappearance of C-H bands at 800 cm^{-1} clearly indicated the elimination of hydrogen. The bands became broader and overlapping due to the strong adsorption of carbon-carbon bonds.

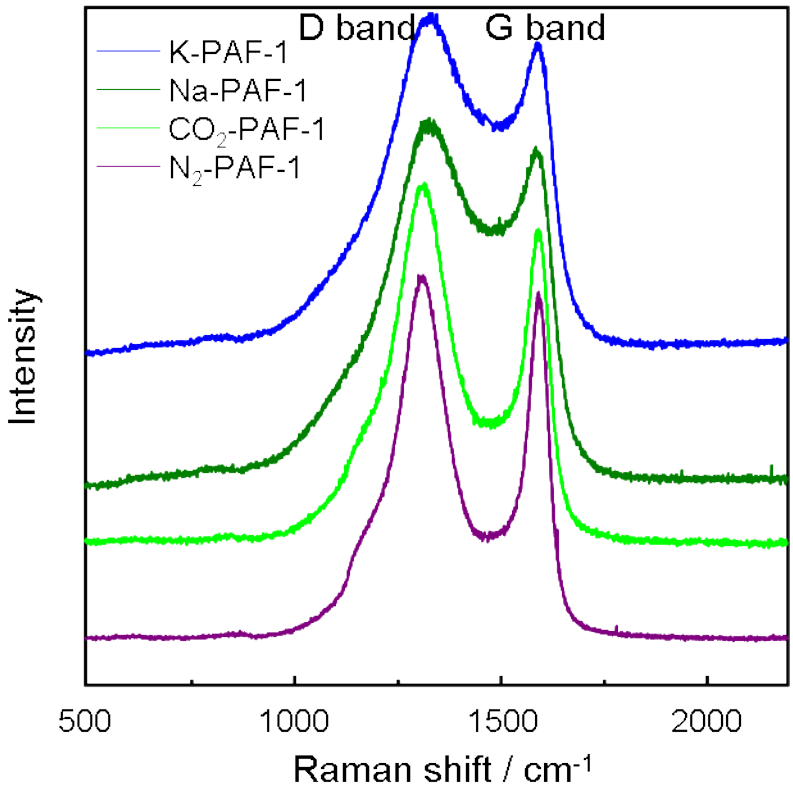

Figure S12. Raman spectra of carbonized samples. The Raman spectra of carbonized PAF-1 showed two Raman shifts, the G-band at 1580 cm^{-1} is associated with the E_{2g} mode of graphite, whereas the D-band centered at around 1380 cm^{-1} is attributed to the D-band of disordered carbon, corresponding to the defect-induced mode. The intensity of the D-band to G-band ratio (I_D/I_G) was in the range of 1.00-1.04, indicating a low degree of graphitization.

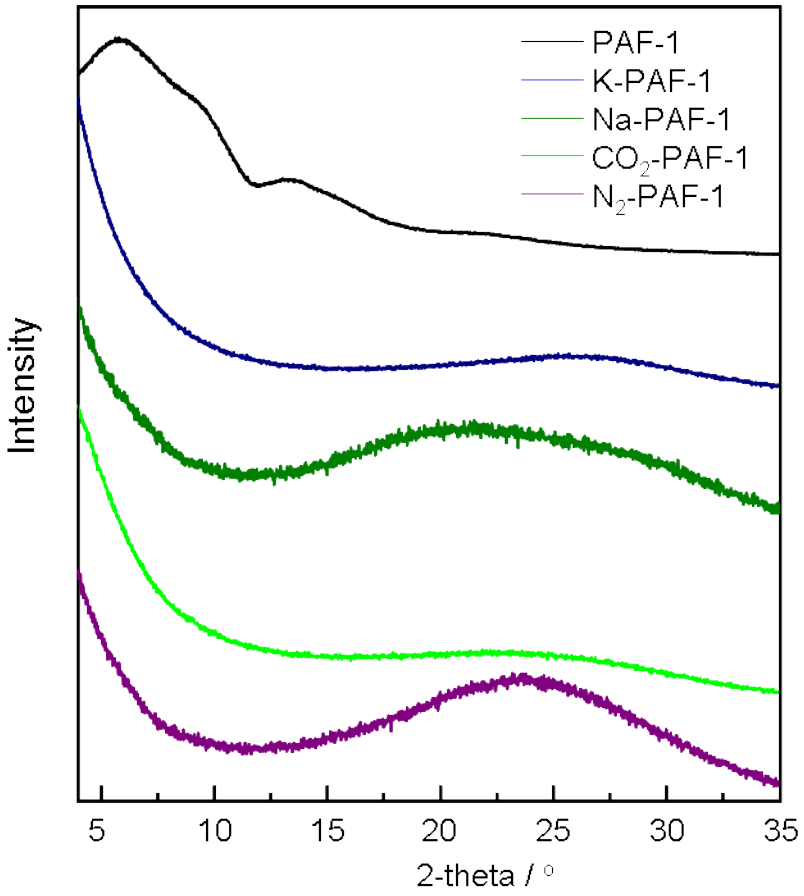

Figure S13. PXRD patterns of PAF-1 and the carbonized samples. The broad peak at 24° for carbonized samples is ascribed to the (002) diffraction of carbon. The broad peak indicated that the carbonized PAFs were essentially amorphous.

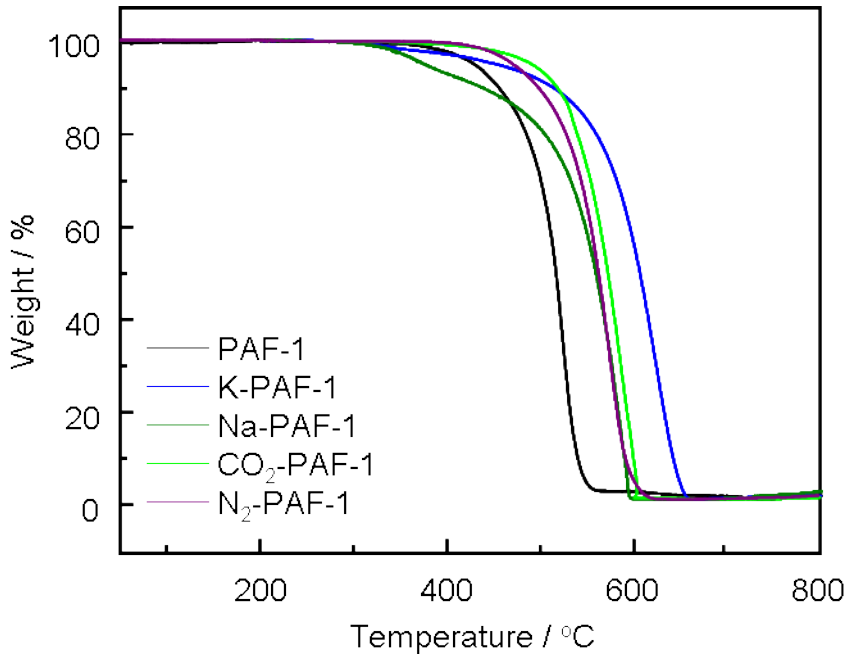

Figure S14. TGA of PAF-1 and the carbonized samples. All the samples do not loss weight before 400 °C, indicating excellent thermal stability.

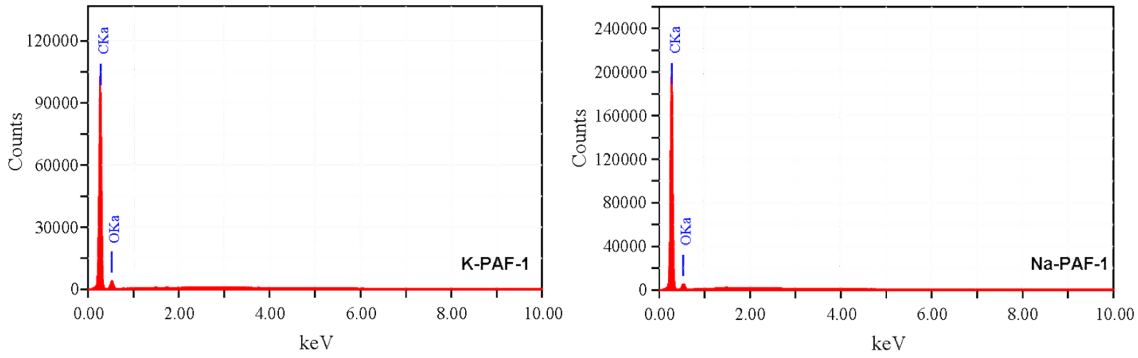

Figure S15. EDS spectra of KOH and NaOH activated samples. It can be seen that no potassium left in the carbon framework.

Table S1. Texture properties of PAF-1 and KOH activated samples at different temperatures.

	Texture properties					
sample	S^{a}_{BET}	Pore size	V_{total} [c]	$V_{0\text{-}1}$ [d]	V_{micro} [e]	V_{meso} [f]
	(m^2g^{-1})	(nm)[b]	(cm^3g^{-1})	(cm^3g^{-1})	(cm^3g^{-1})	(cm^3g^{-1})
PAF-1	5300	1.4	2.43	0.17	1.44	0.99
K-PAF-1-600	2325	0.61 1.20	1.10	0.54	0.88	0.22
K-PAF-1-750	2926	0.79 1.30	1.45	0.46	1.14	0.31
K-PAF-1-800	2857	1.00 （broad）	1.44	0.44	1.11	0.33

a. S_{BET} was calculated in the partial pressure (p/p_0) range of 0.01 to 0.1 which gives the best liner. b. Maxima of the pore size distribution calculated from nitrogen sorption using the QSDFT method and slit-shaped pores. c. Total pore volume at relative pressure p/p_0 = 0.99. d Microporosity attributed to pores less than 1 nm. e. Microporous pore volume for pore less than 2 nm determined. f Mesopore pore volume attributed to pore larger than 2 nm.

Table S2. Element analysis of carbonized samples.

samples	**Element content**		
	C	**H**	**N**
K-PAF-1	**91.69**	**0.44**	**< 0.3**
Na-PAF-1	**85.12**	**1.78**	**< 0.3**
CO_2-PAF-1	**84.76**	**0.78**	**< 0.3**
N_2-PAF-1	**84.52**	**1.08**	**< 0.3**